

# Witt's hyperbola is both predicted and observed to pass close to the lensing galaxies in quadruple quasars

PAUL L. SCHECHTER<sup>1</sup> AND RICHARD LUHTARU<sup>2</sup>

<sup>1</sup>*MIT Kavli Institute and Department of Physics & MIT Kavli Institute McNair Building 37-635, 77 Massachusetts Ave, Cambridge, MA, 02139, USA*

<sup>2</sup>*MIT Department of Physics Cambridge, MA 02139, USA*

## ABSTRACT

When a rectangular hyperbola is constructed from the image positions of a quadruply lensed quasar, as proposed by Witt (1997), it passes very close to the the lensing galaxy. The median measured perpendicular offset between the observed light center of the lens and Witt's hyperbola is  $0''.013$  for a sample for 39 systems lensed by a relatively isolated galaxy. The family of lens models adopted by Witt predicts that the lens lies on the hyperbola, but its position is not used for its construction. The median offset corresponds to roughly 1% of the Einstein ring radius, and suggests that the centers of the lensing potential are close to the light centers of the lens. By putting a restrictive prior on the perpendicular distance to Witt's hyperbola (or on the distance between the galaxy and the potential), one reduces by one the dimensionality of a model space when fitting data. Taking the brightest pixel of a lensing galaxy as its center avoids a shortcoming of using the average light center for a constraint.

*Keywords:* Strong gravitational lensing (1643), Quasars (1319)

## 1. ELIMINATE FREE PARAMETERS WHEN YOU CAN

Any model for a quadruply lensed quasar (or supernova) includes both a model for the lensed object (a pointlike quasar, and sometimes an extended host) and a model for the gravitational potential that deflects light from the source. However small the number of parameters associated with any particular model, one would almost always choose to eliminate a free parameter if it were possible without introducing an unmanageable systematic error.

We argue here that, for the case of relatively isolated lensing galaxies, the observed position of the lensing galaxy can be used to reduce, in effect, the number of model parameters by one. There are roughly a half dozen independent codes used to model quadruply lensed quasars. Most of them use the position of the lensing galaxy to constrain the center of the lensing potential, albeit with differences in implementation. The stringency adopted for these constraints varies from one modeler to the next, with little or no discussion of the choice. And with a few exceptions exceptions e.g.

Chen et al. (2019) there is likewise no reporting of the derived offset of the lens potential from the lensing galaxy.

Here we urge constraining the center of the lens potential using the observed distance of the lensing galaxy from the rectangular hyperbola constructed by Witt (1996), using *only* the positions of the four lensed quasar images and *not* that of the lensing galaxy. While Witt’s recipe is strictly geometric, it was derived from family of physical models that *do* put the center of the lensing potential on his hyperbola. The observed proximity of relatively isolated lenses to Witt’s hyperbola strongly suggests that the the centers of the lensing potentials are likewise close to the hyperbola.

In Section 2 below we review key aspects of Witt’s hyperbola. In Section 3 we report our principal result: for a sample of 39 relatively isolated lensing galaxies, the distances of their observed centers from Witt’s hyperbola are small compared to the systems’ Einstein ring radii. This suggest a prior for use in modeling similar systems. In Section 4 we interpret our measured distances, contending that the family of models that motivated Witt is a good first approximation for systems with a single dominant lens. In an Appendix, we advocate using the brightest point at the center of the lens in calculating offsets from Witt’s hyperbola.

## 2. WITT’S GEOMETRICALLY CONSTRUCTED HYPERBOLA

Witt (1997) showed that *any* gravitational lens whose equipotentials are concentric similar ellipses (characterized here by their semi-ellipticity  $\eta$ ) produces four images that lie on a rectangular hyperbola, one with perpendicular asymptotes. As a special case, Witt’s hyperbola passes through the images produced by singular isothermal elliptical potential (hereafter SIEP).

In addition, Witt showed that a singular isothermal circular potential with external shear,  $\gamma_{ext}$ , (hereafter SIS+XS), *also* produces four images that lie on a rectangular hyperbola.

Moreover there is a one dimensional family of combinations of the SIS+XS and SIEP with shear parallel to ellipticity (henceforth SIEP+XS<sub>||</sub> for all of whose members Witt’s hyperbola passes through the same quartet of observed quasar image positions, contingent on  $\gamma_{ext} + \eta$  being kept constant at some value governed by those  $\gamma_{ext} + \eta$  being kept constant at some value governed by those four positions.

While all of the members of a family with the same value of  $\gamma_{ext} + \eta$  produce the same four quasar images, the position of the center of the potential (which also lies on the hyperbola) varies with the relative importance of  $\gamma_{ext}$  and  $\eta$ . This is extensively delineated by Luhtaru et al. (2021).

Though Witt’s hyperbola was motivated by the SIEP and SIS+XS models, the construction of Witt’s hyperbola depends *only* on the positions of the four quasar images. It is a geometric construct, and with hindsight might have been created without reference to either of those models.

Figure 1 shows Witt hyperbolae overlayed on HST F814W exposures of a dozen lens systems, in all but one of which the lensing galaxy is relatively isolated. The positions of the four quasar images have been used in Witt’s geometric construction but the position of the lensing galaxy has *NOT*. The lensing galaxy nonetheless lies very close to the “primary” branch of the Witt hyperbola in every case. In the next section we quantify this qualitative observation.

## 3. OBSERVED PERPENDICULAR DISTANCES OF RELATIVELY ISOLATED LENS GALAXIES FROM WITT’S HYPERBOLA

### 3.1. What makes quadruply lensed quasars quadruple?

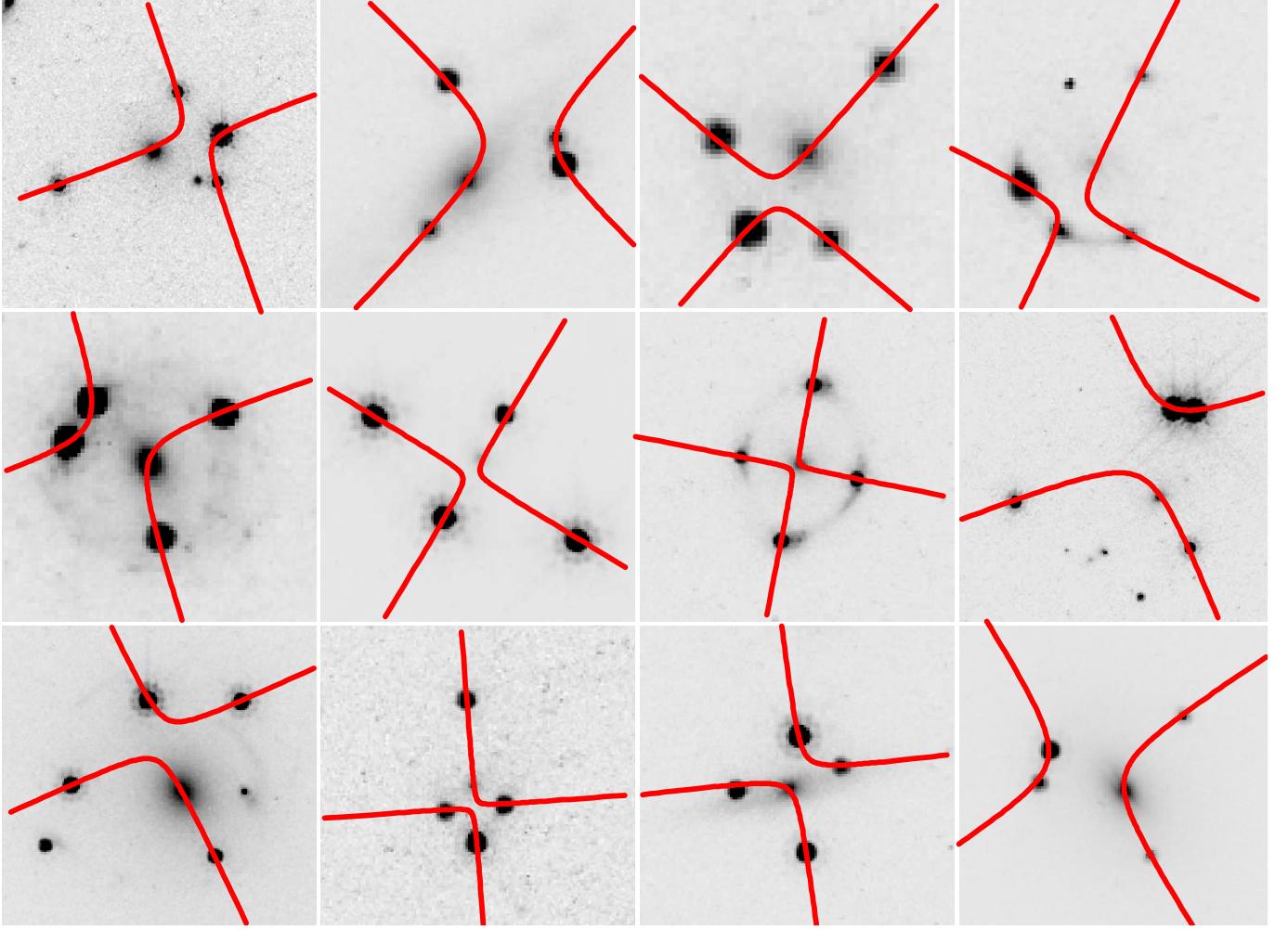


**Figure 1.** Witt’s hyperbola constructed from the four quasar image positions for a dozen systems lensed by galaxies that, in all but one case, are relatively isolated. They were observed with the F814W filter in an HST cycle 26 proposal and are shown superposed on those exposures. The positions of the lensing galaxies were *not* used in constructing the hyperbolae. The long, “primary” branch of the Witt hyperbola nonetheless passes very close to the lensing galaxy in every case, as predicted by the family of models that motivated its construction. Left to right and top to bottom are the systems J0659+16, J1330+18, J2205−37, J1042+16, J1131−44, J1134−21, J1537−30, J0818−26, J1721+88, J0029−38, J1817+27, and J2100−44

[Luhtaru et al. \(2021\)](#) measured perpendicular distances of 39 relatively isolated lens galaxies to Witt’s hyperbola. Those measurements were a byproduct of their primary objective, to answer the question asked in the title of their paper, “What Makes Quadruply Lensed Quasars Quadruple?” They adopted the SIEP + XS<sub>||</sub> family of models introduced in the previous section to determine the relative contributions of shear and semi-ellipticity to the lensing potentials.

In Appendix A we reanalyze 10 of the 39 systems. The incidental perpendicular distances reported there are the focus of the results of the next subsection. For the sake of completeness, we review here some details of the SIEP + XS<sub>||</sub> family of models.

The dimensionless projected potential,  $\psi$  of the SIEP + XS<sub>||</sub> model is given by

$$\psi(b, \eta, \gamma_{ext}) = b \sqrt{q_{pot} x^2 + \frac{y^2}{q_{pot}}} - \frac{\gamma_{ext}}{2} (x^2 - y^2). \quad (1)$$

where  $b$  is the strength of the lens, and  $\gamma_{ext}$  is the shear. [Luhtaru et al. \(2021\)](#) define a “semi-ellipticity”,  $\eta$ , such that

$$q_{pot} = (1 - \eta)/(1 + \eta) \quad , \quad (2)$$

and an “effective quadrupole”,  $\Gamma_{eff}$ ,

$$\Gamma_{eff} \equiv \frac{\gamma_{ext} + \eta}{1 + \gamma_{ext} + \eta} \quad , \quad (3)$$

in which  $\gamma_{ext}$  and  $\eta$  are interchangeable. For semi-ellipticities and shears typical of quadruply lensed quasars

$$\Gamma_{eff} \approx \eta + \gamma_{ext} \quad . \quad (4)$$

The effective quadrupole,  $\Gamma_{eff}$ , is tightly constrained by the elongation of the image configuration. The strength parameter  $b$ , roughly equal to the Einstein radius,  $\theta_E$ , is also well constrained by the four quasar images. By contrast, the ratio of the semi-ellipticity  $\eta$  to the shear,  $\gamma_{ext}$  is unconstrained, by construction,

That ratio *can*, however, be estimated by drawing a line from lensing galaxy perpendicular to Witt’s hyperbola. The position along Witt’s hyperbola determines the ratio. The perpendicular distance,  $D_{\perp}$ , is a byproduct that is central to the present paper.

### 3.2. Observed perpendicular distances from Witt’s hyperbola

The data presented in Table 2 of [Luhtaru et al. \(2021\)](#) were used to determine perpendicular distances for the galaxies in their sample with the exception of the 10 galaxies considered in [A](#) for which our new measurements have been used. In Table 1 we give perpendicular distances from the lens to Witt’s hyperbola for these systems.

**Table 1.** Observed distance of lensed galaxy from Witt’s hyperbola for 39 single-lens systems

System name	$D_{\perp} (")$	System name	$D_{\perp} (")$	System name	$D_{\perp} (")$	System name	$D_{\perp} (")$
J0029-3814	0.011	B0712+472	0.001	SDSS J1251+2935	0.005	J1721+8842	0.016
J0030-1525	0.002	HS0810+2554	0.015	HST12531-2914	0.009	J1817+27	0.051
PS J0147+4630	0.063	RXJ0911+0551	0.001	SDSS J1330+1810	0.005	WFI2026-4536	0.013
SDSS J0248+1913	0.005	SDSS0924+0219	0.000	HST14113+5211	0.022	DES J2038-4008	0.006
ATLAS J0259-1635	0.020	J1042+1641	0.035	H1413+117	0.033	B2045+265	0.014
DES J0405-3308	0.014	PG1115+080	0.007	HST14176+5226	0.075	J2100-4452	0.014
DES J0420-4037	0.002	RXJ1131-1231	0.036	B1422+231	0.007	J2145+6345	0.062
HE0435-1223	0.008	J1131-4419	0.004	SDSS J1433+6007	0.071	J2205-3727	0.000
J0530-3730	0.017	J1134-2103	0.042	J1537-3010	0.004	WISE J2344-3056	0.001
J0659+1629	0.077	SDSS1138+0314	0.004	PS J1606-2333	0.033		

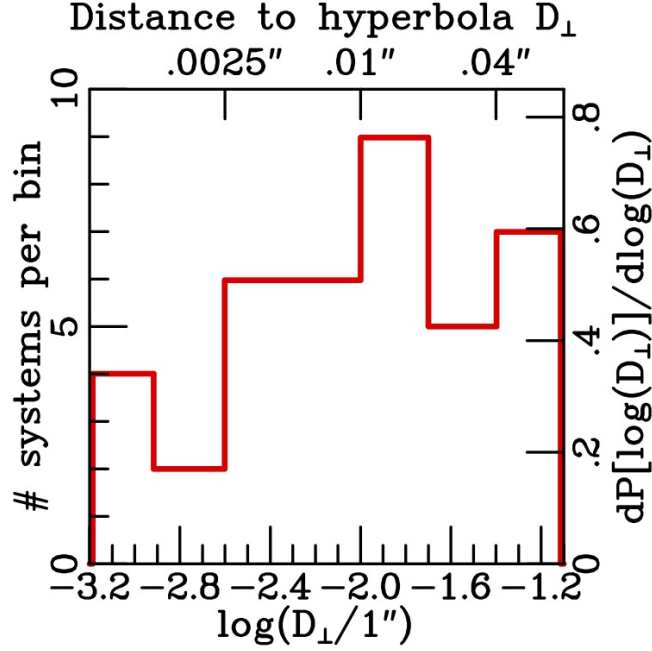


**Figure 2.** The distribution of perpendicular distances,  $D_{\perp}$ , to Witt’s hyperbola measured for the [Luhtaru et al. \(2021\)](#) sample of 39 quasars quadruply lensed by relatively isolated galaxies. The scale on the left gives the number of systems in each bin. The bins have constant logarithmic width  $d\log(D_{\perp}/1'') = \log 2$ , so that each bin spans a factor of two, as shown by the top scale. The scale on the right gives the differential probability  $dP[\log(D_{\perp})]$  of  $\log(D_{\perp})$  per logarithmic increment and integrates to unity over the range shown.

The results of these measurements are presented as a histogram in Figure 2. There are two sets of labels for each axis. The upper axis gives the perpendicular distance,  $D_{\perp}$  in arcseconds. The lower axis gives the decimal logarithm of  $D_{\perp}$ . The 7 bins in the histogram are logarithmic, with  $\Delta D_{\perp} = 0.301$ , corresponding to a factor of two. The left hand axis gives the number of systems in each bin.

As discussed in Appendix A, we estimate the errors in our measured galaxy positions to be *roughly*  $0''.005$ . Those errors dominate the  $D_{\text{perp}}$  measurements on the left half of the histogram. But their contribution to the  $D_{\text{perp}}$  measurements on the right half are likely to be small. We take the  $D_{\perp}$  measurements on the right half of the histogram to reflect shortcomings in the SIEP+XS<sub>||</sub> model.

The right hand axis of Figure 2 gives the differential probability  $dP$  of finding a member of the sample per unit common logarithm,  $d\log(D_{\perp})$ . One obtains it by dividing the number of systems observed in a bin by the sample size, 39, and scaling by  $1/\log 2$ , since we have used bins that span only a factor of two in  $D_{\perp}$ . Using this axis the red curve integrates to unity. Given the small numbers, one might with equanimity summarize the result of Figure 2 as  $dP[\log(D_{\perp})]/d\log(D_{\perp}) = 1/2$  over the range plotted..

It should be noted that average lens strength  $b$  for the seven systems in the rightmost bin is  $<b> = 1''.5$ . One would have a yet tighter constraint if one put a prior on  $D_{\perp}/b$ .

It should also be remembered that the leftmost bins are dominated by errors in the measurement of galaxy centers, which are likely to be different for different data sets.

#### 4. A PRIOR ON THE CENTER OF THE LENSING POTENTIAL

The median  $D_{\perp}$  in Figure 2 is 0''.013. The median value of the lens strength,  $b$ , is 0''.85. This puts the typical lensing galaxy at a distance from Witt's hyperbola that is 1/70th radius of the Einstein ring.

##### 4.1. *What explains the proximity of Witt's hyperbola to the lensing galaxy?*

There are two categories of explanations for the proximity of the lensing galaxy to Witt's hyperbola in Figure 2. The first of these posits that the SIEP+XS<sub>||</sub> is essentially correct and that the center of the potential does in fact lie on Witt's hyperbola. In this case the lensing galaxy is offset from the center of the potential, much as the centers of brightest cluster galaxies are offset from the the centers of their potentials (Skibba et al. 2011).

The second category assumes that the potential *is* centered on the lensing galaxy, but that it is more complicated than SIEP+XS<sub>||</sub> model. The positions of the four quasar images are therefore displaced from the SIEP+XS<sub>||</sub> predictions and a hyperbola that is consequently displaced from the center of the potential. Examples would be equipotentials for which either the ellipticity or their orientation changes as a function of radius.

##### 4.2. *Constraining the center of the lensing potential*

For the first category of explanations, the distribution of offsets shown in Figure 2 is an appropriate prior on the center of the potential for use in modeling quads.

For the second category of explanations, the appropriate prior on the offset of the center of the potential from the center of the lens is a delta function. On the assumption that both explanations are at work, the prior derived from Figure 2 is *conservative*. We recommend its use in modeling quadruply lensed quasars.

Taking the explanation of the offsets of the lens of the potential to arise entirely from unmodeled complexities in the true potential (category 1), modelers can still use the perpendicular distances in 2 even if they are disinclined to adding this term in the quantity they minimize. One can assume that those complexities introduce an offset of the hyperbola from point where the perpendicular intersects in the direction orthogonal to the perpendicular that is equal to the perpendicular offset. Multiplying the abscissas in Figure 2 by  $\sqrt{2}$ , the figure can be taken as a prior on the offset of the center of the potential from the center of light.

#### 5. CONCLUSIONS

We have shown when a relatively isolated galaxy produces a quadruply lensed quasar, its center lies close to the hyperbola constructed by Witt (1996) from the positions of the four quasar images. This permits the use of a strong prior the position of the center of the lensing potential. in effect reducing by one the number of parameters model parameters used to model such a system.

We thank Sebastian Ertl for communicating results in advance of publication. We also thank an anonymous referee for a careful reading that led to a complete overhaul of the paper, from title to conclusions.



## APPENDIX

## A. NEW MEASUREMENTS OF THE CENTERS OF GALAXIES QUADRUPLY LENSING QUASARS

A.1. *Why does the astrometric accuracy of lens positions matter?*

We did not set out to study the proximity of lensing galaxies to Witt’s hyperbola reported in Section 3.2. That finding emerged from an effort to improve upon the estimate of the relative contributions of the flattening of lens galaxies on one hand and tidal shear on the other to the quadrupole moments of potentials obtained by Luhtaru et al. (2021), whose approach is described in Section 3.1.

Their scheme is limited by the accuracy with which one can measure the positions of the quasar images and the position of the lensing galaxy, which is assumed to have a singular isothermal elliptical potential with parallel external shear (the SIEP+XS<sub>||</sub> model). The uncertainty in the flattening/shear decomposition is estimated from the offset the lensing galaxy from the Witt (1996) hyperbola.

Luhtaru et al. concluded that shear contributes roughly twice as much as galaxy flattening to the “effective shear”,  $\Gamma_{eff}$ , the overall quadrupole component of a potential that quadruply lenses a quasar. Were the uncertainties in their adopted positions larger than reported, the reliability of that conclusion might be challenged.

Measuring positions for the four images of a quadruply lensed quasar is less straightforward than one might at first imagine. The quasars are embedded in host galaxies and their images are projected onto the lensing galaxies. Perfect modeling of an exposure must take into account the point spread function, the various shapes and sizes of galaxies (lenses and quasar hosts), and the gravitational potential that produces four images from a single quasar and host. While multiple software suites are widely available to analyze quadruply lensed quasar systems, each of them incorporates different choices in accounting for the relative importance of these features.

A.2. *Discrepant reports of image and lens center positions*

Ertl et al. (2023) compared positions for the images of nine quadruply lensed quasars measured using two different automated schemes on the same set of HST images. One of those was a version of **Lenstronomy** developed by Schmidt et al. (2023) and described therein. The other was a version of **GLEE**, developed and described by Ertl et al. (2023)

After discarding one extremely discrepant system, in the quasar image positions measured using the two schemes differed by 0″006 and 0″005 in right ascension and declination. This was larger than had been anticipated. Comparing the GLEE results with astrometry from Gaia DR3 (Gaia Collaboration et al. 2021), Ertl et al. reported differences of 0″0017 and 0″0023, respectively.

Luhtaru et al. (2021) was based on astrometry drawn from the literature, much of it from the CASTLES (Kochanek et al. 1999) data base. They also reported new measurements on thirteen recently acquired HST exposures. They described their measurements, using a program called **clumpfit**, as “preliminary” deferring to the anticipated measurements by Schmidt et al. (2023) which they called “authoritative.” When Ertl et al. compared their GLEE astrometry with the “preliminary” results of Luhtaru et al. (2021), they found rms differences marginally smaller than with Gaia DR3, 0″0017 in each direction. It would therefore seem that Luhtaru et al. were mistaken in deferring to the Schmidt et al. (2023) measurements.

Luhtaru et al. originally used measurements for ten systems reported by Shajib et al. (2019) that were obtained with an earlier version of `lenstronomy`.<sup>1</sup> If the errors in these were as large as those in the Schmidt et al. (2023) astrometry, the Luhtaru et al. conclusion regarding the relative importance of shear and ellipticity might be compromised. We therefore remeasured, using `clumpfit`, the same ten HST images analyzed by Shajib et al. (2019).

In comparing `clumpfit` and GLEE, we were impressed that the agreement for some systems was better than  $0''.001$ . With positions this good, the uncertainties in the modeled centers of the potentials would be correspondingly accurate. This motivated us to compare the `clumpfit` positions for the maximum in lens surface brightness with the theoretical centers for the potential computed from the positions of the quasar images.

### A.3. New `clumpfit` astrometry

The Luhtaru et al. (2021) measurements were carried out with the program `clumpfit` described briefly in Agnello et al. (2018). It incorporates elements of DoPHOT (Schechter et al. 1993), fitting point sources with either an elliptical “pseudo-Gaussian” or a lookup table taken from a nearby star. Galaxies are fit with elliptical pseudo-Gaussians. These do not allow for curved images and so are ill suited toward modeling the images of quasar hosts. The `clumpfit` model does not couple the images to a lensing potential, which can be modeled subsequently using the image parameters.

We used nearby stars as PSF templates when possible. Unfortunately, for the majority of systems there were no stars on the HST images sufficiently bright for this purpose, so pseudo-Gaussians were used. For some of the systems for which PSF templates were available we also tried pseudo-Gaussians and found no substantial differences.

The position of the lensing galaxy is of primary importance in distinguishing between ellipticity and shear, so the `clumpfit` residuals were examined for effects that might influence the position of the lensing galaxy.

The two greatest concerns were that a) the very substantial residuals from the four point sources would “pull” or “push” the outer isophotes of the much lower surface brightness lensing galaxy and b) that the unmodeled flux from the quasar host might similarly pull those isophotes.

To minimize this effect, the lensing galaxy was often taken to be smaller than its isophotes would indicate, so as to weight the light from the center of the lens more heavily. In some cases, the width of the pseudo-Gaussian model was fixed at a value smaller than the best fitting value. In others, the lens galaxy was taken to have the PSF of a stellar template. Either way, the central intensity of the model for the starlight was adjusted by hand to exactly account for the flux at the center of the lens.

The effect is illustrated in Figure 3, which shows results from two alternative fits of surface brightness profiles to an HST F814 image of the lensed quasar system J1251+29. The left panel shows residuals when stellar PSFs are fit to the four images and the central galaxy is taken to be a unconstrained elliptical pseudo-Gaussian. Note that the galaxy has been pulled toward the extended structure of the quasar host, leaving positive residuals at the center of the lensing galaxy and negative residuals toward the triplet of quasar images. Using this fit, Luhtaru et al. (2021) found the system to be shear-dominated.

<sup>1</sup> Luhtaru et al. (2021) chose to use astrometry for an eleventh system, SDSS1310+18, from Rusu & Lemon (2018) rather than that of Shajib et al. (2019).



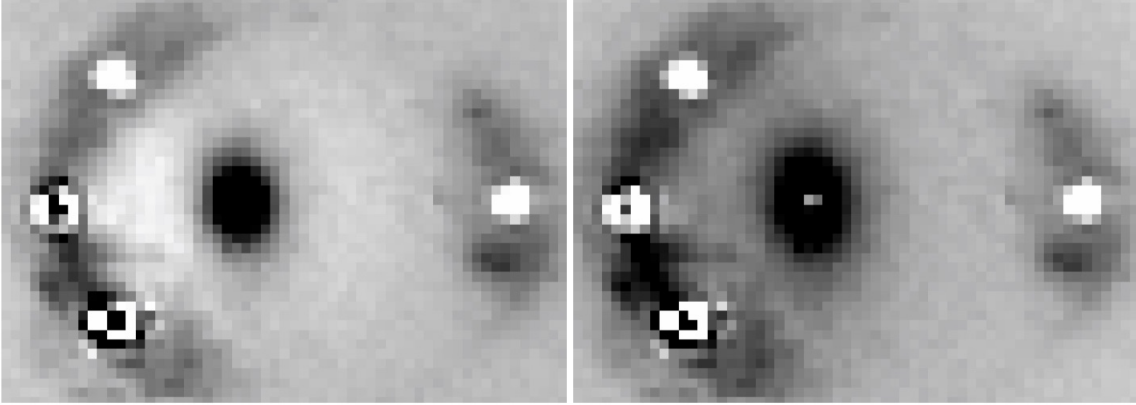


**Figure 3.** The left and right panels show residuals at the same contrast from fits of two different models to an HST F814W exposure of J1251+29. In the left panel, the lensing galaxy was taken to be an elliptical pseudo-Gaussian. In the right panel, it was taken to be a point source producing zero residual flux in the central pixel. The residuals in the left panel are asymmetric, the result of the outer isophotes of the elliptical Gaussian being pulled toward the extended structure of the quasar host.

The right panel shows residuals from the fit of the stellar PSF to the center of the galaxy, with the amplitude constrained to give zero residual in the brightest pixel. The resulting center is our best estimate of the true position, giving shear and ellipticity contributing equally. This result is still somewhat suspect, as the angle of the resultant quadrupole lies very close to the position angle of the isophotes of the lensing galaxy.

The lesson to be learned (or reinforced) from Figure 3 is that residuals tell you more than side-by-side comparisons of models and data.<sup>2</sup>

As we worked through the sample, system by system, to improve upon the derived centroids, different schemes were developed on an ad hoc basis. The effects of imperfect point source subtraction on the lens position could in some cases be minimized by measuring an F475X exposure rather than the F814W exposure, but we this was done only when the F814W frame gave a suspect result. For some systems the lensing galaxy was too faint to make the F475X exposure useful. Each of the ten systems for which we present results was therefore treated slightly differently, depending upon the particular circumstances.

Our new astrometric measurements for the ten quadruply lensed quasars for which Luhtaru et al. (2021) differentially adopted those of Shajib et al. (2019) are presented in Table 2. The agreement between the “provisional” ad hoc *clumpfit* astrometry of Luhtaru et al. (2021) and the GLEE astrometry of Ertl et al. (2023) was unexpectedly good. If we assume that the two programs contribute equally to the rms differences in the quasar astrometry, we get errors of of  $0''.0013$  in each coordinate. We have therefore included a fourth decimal place in Table 2.

#### A.4. Confirmation of shear dominance

In Table 3 we give shear/ellipticity decompositions for our 10 newly measured systems that, for the reasons elaborated above, we believe are more reliable than those in Table 2 of Luhtaru et al. (2021).

<sup>2</sup> Secondly, white sky (inverse grayscale) representations do better at bringing out low surface brightness residuals.

**Table 2.** Newly measured relative positions for galaxies and images of quadruply lensed quasars

System name	Image A		Image B		Image C		Image D		Galaxy	
	$\Delta\alpha \cos \delta$	$\Delta\delta$	$\Delta\alpha \cos \delta$	$\Delta\delta$	$\Delta\alpha \cos \delta$	$\Delta\delta$	$\Delta\alpha \cos \delta$	$\Delta\delta$	$\Delta\alpha \cos \delta$	$\Delta\delta$
	(")	(")	(")	(")	(")	(")	(")	(")	(")	(")
PS J0147+4630	0.0000	0.0000	1.1697	-0.4141	-1.2404	-0.0993	-0.3394	-3.2351	-0.1650	-2.0671
SDSS J0248+1913	0.0000	0.0000	-0.1472	-0.8344	0.8543	-1.4463	0.9050	-0.0366	0.4905	-0.6361
ATLAS J0259-1635	0.0000	0.0000	-0.3192	0.8789	-1.4736	0.5647	-0.7163	-0.3845	-0.6812	0.2950
DES J0405-3308	0.0000	0.0000	-1.0656	-0.3261	-0.3416	0.8332	-1.2232	0.6967	-0.7007	0.2364
DES J0420-4037	0.0000	0.0000	0.2432	1.0271	0.8732	1.1431	1.4018	-0.2268	0.6938	0.3468
SDSS J1251+2935	0.0000	0.0000	0.2913	0.9626	0.3581	0.3756	-1.4249	0.9553	-0.3459	0.6239
SDSS J1433+6007	0.0000	0.0000	2.0455	1.5804	0.0017	3.7554	-0.7599	1.6262	0.9332	1.7008
PS J1606-2333	0.0000	0.0000	-1.6211	-0.5888	-0.7919	-0.9052	-1.1278	0.1504	-0.8345	-0.3669
DES J2038-4008	0.0000	0.0000	1.5128	-0.0274	1.3873	2.0594	-0.7923	1.6769	0.6779	1.1833
ATLAS J2344-3056	0.0000	0.0000	-0.2915	0.6696	-0.8744	0.3207	-0.6332	-0.3364	-0.4173	0.1515

**Table 3.** Shear ellipticity decompositions for 10 newly measured systems

System name	$\gamma$	$\eta$	$\Delta\gamma$	$\Gamma_{eff}$	System name	$\gamma$	$\eta$	$\Delta\gamma$	$\Gamma_{eff}$
PS J0147+4630	0.180	-0.020	0.017	0.160	SDSS J1251+2935	0.053	0.053	0.005	0.105
SDSS J0248+1913	0.120	-0.020	0.012	0.100	SDSS J1433+6007	0.197	0.001	0.038	0.198
ATLAS J0259-1635	0.031	0.038	0.062	0.069	PS J1606-2333	0.234	-0.026	0.139	0.209
DES J0405-3308	-0.011	0.034	0.051	0.023	DES J2038-4008	0.035	0.056	0.007	0.091
DES J0420-4037	0.000	0.034	0.004	0.034	ATLAS J2344-3056	-0.168	0.232	0.016	0.067

While individual entries differ, replacement of the corresponding entries in Table 2 of [Luhtaru et al. \(2021\)](#) with the values in Table 3 gives no substantial change in the conclusion that shear dominates ellipticity by roughly a factor of 2:1. This confirmation of the Luhtaru et al. result would have been the conclusion of the paper that we originally intended to write, but it seemed less consequential than the proximity of the lensing galaxies to Witt’s hyperbola that we address in the main body of this paper.

## REFERENCES

- Agnello, A., Schechter, P. L., Morgan, N. D., et al. 2018, *MNRAS*, 475, 2086, doi: [10.1093/mnras/stx3226](https://doi.org/10.1093/mnras/stx3226)
- Chen, G. C. F., Fassnacht, C. D., Suyu, S. H., et al. 2019, *MNRAS*, 490, 1743, doi: [10.1093/mnras/stz2547](https://doi.org/10.1093/mnras/stz2547)
- Ertl, S., Schuldt, S., Suyu, S. H., et al. 2023, *A&A*, 672, A2, doi: [10.1051/0004-6361/202244909](https://doi.org/10.1051/0004-6361/202244909)
- Gaia Collaboration, Brown, A. G. A., Vallenari, A., et al. 2021, *A&A*, 649, A1, doi: [10.1051/0004-6361/202039657](https://doi.org/10.1051/0004-6361/202039657)
- Kochanek, C. S., Falco, E. E., Impey, C., et al. 1999, CASTLES Gravitational Lens Data Base. <https://www.cfa.harvard.edu/castles/>
- Luhtaru, R., Schechter, P. L., & de Soto, K. M. 2021, *ApJ*, 915, 4, doi: [10.3847/1538-4357/abfda1](https://doi.org/10.3847/1538-4357/abfda1)

- Rusu, C. E., & Lemon, C. A. 2018, Research Notes of the American Astronomical Society, 2, 187, doi: [10.3847/2515-5172/aae5f1](https://doi.org/10.3847/2515-5172/aae5f1)
- Schechter, P. L., Mateo, M., & Saha, A. 1993, PASP, 105, 1342, doi: [10.1086/133316](https://doi.org/10.1086/133316)
- Schmidt, T., Treu, T., Birrer, S., et al. 2023, MNRAS, 518, 1260, doi: [10.1093/mnras/stac2235](https://doi.org/10.1093/mnras/stac2235)
- Shajib, A. J., Birrer, S., Treu, T., et al. 2019, MNRAS, 483, 5649, doi: [10.1093/mnras/sty3397](https://doi.org/10.1093/mnras/sty3397)
- Skibba, R. A., van den Bosch, F. C., Yang, X., et al. 2011, MNRAS, 410, 417, doi: [10.1111/j.1365-2966.2010.17452.x](https://doi.org/10.1111/j.1365-2966.2010.17452.x)
- Witt, H. J. 1996, ApJL, 472, L1, doi: [10.1086/310358](https://doi.org/10.1086/310358)